

Experimental and simulative investigation of flame–wall interactions and quenching in spark-ignition engines

Dominik Suckart¹ · Dirk Linse² · Eberhard Schutting³ · Helmut Eichlseder³

Received: 19 September 2016 / Accepted: 3 December 2016 / Published online: 22 December 2016
© The Author(s) 2016. This article is published with open access at Springerlink.com

Abstract Flame–wall interactions are a crucial aspect concerning the design and optimisation of a spark-ignition engine. To improve the understanding of the phenomenon, flame–wall interactions are investigated by highly resolved wall heat flux measurements. For this purpose, a turbo-charged, direct-injected spark-ignition engine was equipped with eight surface thermocouples and operated at five measuring points to examine the influence of speed, load, charge motion and equivalence ratio on the quenching process. A cycle-resolved analysis is utilized to extract the wall heat fluxes during flame–wall interaction which are subsequently used to calculate the quenching distances, as well as the normalised wall heat fluxes and Peclet numbers. To correctly estimate these values, a simulative methodology based upon a 3D-CFD in-cylinder flow and a 1D flame calculation with detailed chemical kinetics is employed. The 3D-CFD in-cylinder flow was combined with a 3D-FE heat conduction and 3D-CFD coolant flow simulation to properly predict the wall temperatures and thereby the near-wall flow state. The findings show that the

quenching distance is proportional to the laminar flame thickness at first order. Hence, the engine load is found to be the main parameter influencing the quenching distance. The analysis of the quenching distances, normalized wall heat fluxes and Peclet numbers reveals that flame–wall interactions in spark-ignition engines exhibit strong similarities to laminar premixed flame–wall interactions. In addition, two correlations for calculating the quenching distance are proposed. These insights provide a deeper understanding of flame–wall interactions in spark-ignition engines and can be used to develop or adapt turbulent combustion models.

Keywords Combustion · Flame–Wall interaction · Quenching · Gasoline engine · Spark ignition · Heat flux

Abbreviations

CFD	Computational fluid dynamics
FE	Finite elements
HOQ	Head-on quenching
IMP	Indicated mean pressure
LES	Large Eddy simulation
OP	Operating point
SWQ	Side-wall quenching
URANS	Unsteady Reynolds-averaged Navier–Stokes

List of symbols

α_Q	Crank angle in the moment of quenching
$\dot{Q}_{w,Q}$	Wall heat flux in the moment of quenching
\dot{Q}_Σ	Heat release rate of an undisturbed flame
y_Q	Quenching distance
φ_Q	Normalised wall heat flux
Pe_Q	Quenching Peclet number
p	Pressure

✉ Dominik Suckart
dominik.suckart@bmw-m.com

Dirk Linse
dirk.linse@bmw.com

Eberhard Schutting
schutting@ivt.tugraz.at

Helmut Eichlseder
eichlseder@ivt.tugraz.at

¹ BMW M GmbH, BMW Group, Munich, Germany

² CAE Combustion, BMW Group, Munich, Germany

³ Institute of Internal Combustion Engines and Thermodynamics, Graz University of Technology, Graz, Austria

ϕ	Equivalence ratio
Y_{EGR}	Residual gas mass fraction
T_{b}	Adiabatic flame temperature
T_{u}	Unburnt mixture temperature
T_{W}	Wall temperature
T_0	Inner layer temperature
ρ_{u}	Unburned gas density
λ	Thermal conductivity
c_p	Isobaric specific heat
s_L^0	Adiabatic laminar flame speed
l_{F}	Diffusive flame thickness
$l_{\text{F,CH}_4}$	Diffusive flame thickness of methane-air flames
$l_{\text{F,g}}$	Diffusive flame thickness of gasoline-air flames

1 Introduction

The combustion process of a modern spark-ignition engine plays a key role concerning emissions, efficiency and performance. Its analysis and optimisation requires in-depth knowledge of the underlying physics, as well as comprehensive numerical models and simulation tools. In the past, considerable attention was given to the ignition process (e.g. Dahms et al. [16]), main combustion phase (e.g. Linse et al. [26]) or irregular knocking combustion (e.g. Linse et al. [27]). Despite the fact that 60–80% of the in-cylinder charge is burned by a decelerating flame (Heywood [22], Liu et al. [28]), only few publications concentrated on this late stage of combustion where quenching, i.e. flame extinction at cold walls, occurs. The interaction of a (turbulent) flame with the walls of a combustion chamber significantly influences the combustion efficiency, the wall heat losses and to a smaller extent the engine-out HC-emissions (cf. Alkidas [3]). Hence, flame–wall interactions have to be accounted for to optimise the design of an engine. This aspect becomes especially relevant for downsized engines with a high surface-to-volume ratio of the combustion chamber and/or a high power per displacement. Therefore, a thorough understanding of flame–wall interactions in spark-ignition engines is vital.

1.1 Literature review

The quenching of premixed flames received considerable interest by researchers for many decades. It is well-established that the main mechanism leading to flame extinction near cold walls ($T_{\text{W}} < 600 \text{ K}$) is the thermal loss to the wall. Once the flame approaches the wall, the increasing wall heat losses inhibit all reactions with high activation energies, especially chain branching reactions, due to an insufficient temperature level. Only radical recombination reactions are able to take place. The

decreasing radical pool slows down the chain branching reactions even further until the flame is subsequently quenched [21, 34, 35, 40]. It was shown that the wall heat flux reaches its maximum in the moment of quenching and that this value is correlated to the heat release rate of the flame, as well as to the quenching distance y_{Q} (cf. Vosen et al. [38]). Early studies focused on this aspect of flame–wall interactions, since the wall heat flux is relatively simple to measure in contrast to a direct (optical) observation. It was demonstrated that the wall heat flux normalised with the heat release rate of the flame is a characteristic feature of quenching. It remains constant at around 0.3 for head-on quenching for a wide variety of equivalence ratios [18, 23, 38], hydrocarbon fuels [18, 21, 23, 29, 38], pressures [25, 37] and wall temperatures [14, 15, 18, 21, 29, 34]. In a similar manner, the quenching distance can be normalised with the laminar flame thickness l_{F} yielding the second characteristic quantity of flame–wall interactions, the so-called Peclet number $\text{Pe}_{\text{Q}} = y_{\text{Q}}/l_{\text{F}}$, which typically ranges between 3 and 4 for laminar head-on quenching.

In contrast to laminar flame–wall interactions, turbulent flame–wall interactions were studied less extensively albeit their importance for almost any modern combustion system including spark-ignition engines. The reason for this is the complex nature of the phenomenon with many interacting processes. As a consequence, the majority of publications on this topic are numerical studies restricted to generic turbulent flows such as a channel or Couette flow. Bruneaux et al. [9–11] were among the first to carry out a three-dimensional direct numerical simulation of flame quenching in a turbulent channel flow. They found out that flame–wall interactions are influenced by the near-wall structures of the turbulent boundary layer flow, like the hairpin vortex [33]. These vortices can push the flame towards the wall decreasing the quenching distance and increasing the wall heat flux in turn. This observation was later confirmed by Alshaalan et al. [4, 5] for a flame in a turbulent Couette flow. They also remarked that the inverse correlation between the wall heat flux and the quenching distance still holds for turbulent conditions. The first calculation with detailed chemistry was conducted in a turbulent channel flow by Gruber et al. [19]. They determined that the thermal quenching mechanism of laminar flames is also the dominant mechanism for turbulent flames. In both cases, the flame is quenched due to the promotion of radical recombination reactions and inhibition of chain-branching reactions.

1.2 Objective and structure of this work

The question, which arises at this point, is whether these mechanisms apply to flame–wall interactions in

spark-ignition engines. Recent publications [1, 36] suggest that the near-wall turbulence in engines differs from the one found in canonical turbulent flows over flat planes. Most notably, the former does not exhibit a peak of the turbulent kinetic energy near the wall like the latter. This directly leads to the assumption that flame–wall interactions in engines are only weakly influenced by turbulence. It is a common assumption that a relaminarization of the turbulent flame occurs near the walls of a combustion engine (cf. Boust et al. [8]), however, experimental evidence on this phenomenon is scarce. Similarly, there is a considerable shortage of appropriate experimental data (e.g. quenching distances or Peclet numbers) on the quenching process in spark-ignition engines. Therefore, the aim of this study is to analyse and clarify the nature of flame–wall interactions in spark-ignition engines providing guidance and references for future modelling attempts.

For this purpose, the instantaneous wall heat flux at eight positions in the cylinder head of a modern spark-ignition engine was measured using the well-known surface temperature method (e.g. Wimmer et al. [41]). A total of five operating points was investigated to study the influence of engine speed, load, charge motion and equivalence ratio. This allows a comprehensive analysis of flame–wall interactions with respect to a wide range of pressures, temperatures and mixture properties.

Since the flame–wall interaction process is subjected to considerable cycle-to-cycle variations, the analysis of ensemble—averaged wall heat fluxes is insufficient. Hence, a procedure is proposed to extract and analyse the quenching wall heat flux based on single cycles. The estimation of the quenching distance, as well as the Peclet number and the normalised wall heat flux requires the local mixture properties in the combustion chamber in the moment of quenching. For an accurate estimation of these properties, a methodology is developed comprising 3D-CFD, 3D-FE and 1D simulations incorporating detailed chemical kinetics.

The obtained quenching distances are discussed in detail and two relations for its modelling are proposed. The effects of the operating parameters of the engine on the quenching distance are shown. Moreover, an emphasis is laid on a comparison to the data found in literature. The corresponding Peclet numbers and normalised wall heat fluxes are presented subsequently. It is shown that the quenching process in a spark-ignition engine is comparable to laminar flame–wall interactions and mainly influenced by the flame orientation and the local mixture properties in the combustion chamber.

2 Theory

Flame–wall interactions are encountered in almost any technical device with a closed combustion chamber, especially spark-ignition engines. Generally, one can distinguish between three characteristic configurations (Poin-sot and Veynante [32]):

- head-on quenching (HOQ), where the flame front is parallel to the wall and propagates towards it.
- side-wall quenching (SWQ), where the flame front is perpendicular to the wall and propagates parallel to it.
- tube quenching, which describes quenching in tubes with a sufficiently small diameter.

The latter one is only of minor importance considering flame–wall interactions in spark-ignition engines and will not be discussed further. During SWQ, the wall heat flux is generally lower and the quenching process can additionally be influenced by flame stretch increasing the quenching distance (cf. Enomoto [17]). However, flame stretch is commonly a secondary parameter compared to thermal losses (Boust et al. [8]).

In the following, the definitions of the normalised wall heat flux as well as the Peclet number are introduced. Their characteristic magnitudes are discussed and two approaches for the estimation of the quenching distance based on the wall heat flux are presented.

2.1 General definitions

To quantify and assess flame–wall interactions, the wall heat flux in the moment of quenching $\dot{Q}_{w,Q}$ is commonly normalised by the heat release rate of an undisturbed flame \dot{Q}_{Σ} , also called flame power, yielding the normalised wall heat flux φ_Q :

$$\varphi_Q = \frac{\dot{Q}_{w,Q}}{\dot{Q}_{\Sigma}} = \frac{\dot{Q}_{w,Q}}{\rho_u s_L^0 c_p (T_b - T_u)}. \quad (1)$$

The second characteristic quantity, the Peclet number Pe_Q , is calculated by normalising the quenching distance y_Q with the diffusive flame thickness l_F :

$$Pe_Q = \frac{y_Q}{l_F} = \frac{\rho_u c_p s_L^0 \times y_Q}{\lambda} \quad (2)$$

with

$$l_F = \frac{\lambda}{\rho_u c_p s_L^0}. \quad (3)$$

The normalised wall heat flux φ_Q and the Peclet number Pe_Q are inversely related. Boust et al. [6, 8] proposed the following correlation:

$$\text{Pe}_Q = \frac{T_b - T_w}{T_b - T_u} \times \left(\frac{1}{\varphi_Q} - 1 \right). \quad (4)$$

For laminar head-on quenching at ambient conditions, a normalised wall heat flux $\varphi_Q \approx 0.3$ and a Peclet number $\text{Pe}_Q \approx 3 - 4$ are characteristic. However, it was shown by Hasse et al. [21], Sotton et al. [37] and Labuda et al. [25] that φ_Q and Pe_Q are slightly pressure dependant. Hence, the correct choice of these bound is vital for the analysis of flame–wall interactions in a spark-ignition engine. Since the normalised scales behave similar for all hydrocarbon fuels, guidance can be obtained by analysing the study of Labuda et al. [25]. The normalised wall heat flux for laminar head-on quenching of stoichiometric methane-air flames at $p > 20\text{bar}$ and $T_u \approx 850\text{K}$ is approximately $\varphi_Q \approx 0.2$. The corresponding Peclet number can be found using relation (4) and assuming $T_b \approx 2500\text{K}$: $\text{Pe}_Q \approx \frac{2500-415\text{K}}{2500-850\text{K}} \frac{1-0.2}{0.2} \approx 5$. The error concerning the estimate of φ_Q was specified by Labuda et al. [25] to lie within 15–20%. Thus, it can be expected that the wall heat flux during laminar head-on quenching of hydrocarbon flames at elevated pressures varies between $\varphi_{Q,\text{HOQ}} \approx 0.17-0.23$. Correspondingly, the Peclet number can be estimated as $\text{Pe}_{Q,\text{HOQ}} \approx 4-6$.

As already indicated, the quenching distance for SWQ is higher than for HOQ. The data provided in a study by Boust et al. [8] allows the conclusion that the quenching distance for SWQ at slightly elevated pressures is higher by a factor of approximately 2.5 compared to HOQ. This can be complemented by numerical results published by Poinso et al. [31] indicating a factor of around 2. Hence, a sound approximation for the Peclet number during SWQ based on the previously discussed magnitude of $\text{Pe}_{Q,\text{HOQ}}$ is $\text{Pe}_{Q,\text{SWQ}} \approx 10-15$. Similarly, the wall heat flux during side-wall quenching is expected to be smaller by a factor of 2–3 compared to head-on quenching and vary between $\varphi_{Q,\text{SWQ}} \approx 0.06-0.1$.

2.2 Quenching distance estimation

The relation (4) between the normalized wall heat flux and the Peclet number can be used in combination with the definition of the Peclet number (2) to calculate the quenching distance. Several authors validated this procedure against laminar quenching distances of methane-air flames obtained by optical [6–8, 37] and electrical probe diagnostics [24, 25]. However, the definition of the flame position and thereby the quenching distance relied on an optical criterion (chemiluminescence of CH^* and C_2^*) which is difficult to correlate and compare to simulations.

For this reason, an alternative approach is proposed. An obvious relation for the estimation of the quenching distance can be stated as

Table 1 Comparison of sensitivities towards changes in T_u and ϕ of Eqs. (4) and (6)

	Inner layer formulation	Formulation by Boust et al.
$\partial y_Q / \partial T_u$	$5.9 \times 10^{-3} \frac{\mu\text{m}}{\text{K}}$	$2.12 \times 10^{-2} \frac{\mu\text{m}}{\text{K}}$
$\partial y_Q / \partial \phi$	$0.117 \frac{\mu\text{m}}{1/100}$	$0.125 \frac{\mu\text{m}}{1/100}$

$$\dot{Q}_{w,Q} = \lambda \frac{\partial T}{\partial x} \Big|_w \approx \lambda \frac{T_{F,Q} - T_w}{y_Q}, \quad (5)$$

where it is assumed that the heat flux across the chemically inert unburned layer of thickness y_Q is constant in the moment of quenching (cf. Boust et al. [8]). A major drawback of this relation is the unknown temperature $T_{F,Q}$ of the flame during quenching. A physically sound approximation is the inner layer temperature T_0 , due to its significance for kinetically determined flame extinction and flammability limits (cf. Peters [30]). Chain branching and chain terminating reactions are assumed to be in an equilibrium at T_0 . If the flame temperature falls below T_0 , the chain terminating reactions become dominating and the flame eventually extinguishes. An estimate for the quenching distance using the inner layer temperature then reads

$$y_Q = \lambda \frac{T_0 - T_w}{\dot{Q}_{w,Q}}, \quad (6)$$

where λ is estimated at $T = 1/2(T_0 + T_w)$. This formulation, called 'inner layer formulation' in the following, is used besides the relation (4) by Boust et al. to calculate the quenching distances. It is expected that the results of both relations coincide within certain bounds attributed to different modelling assumptions. An important characteristic of the inner layer formulation is that it is less sensitive towards errors in the estimation of the state variables, especially concerning T_u and ϕ . This can be shown by calculating the first-order Taylor series of y_Q estimated with Eq. (4) respectively (6) around a pre-defined 'operating point' representative for the investigated experimental conditions. For the present example, this point is chosen as $p = 60\text{bar}$, $T_u = 800\text{K}$, $\phi = 1.0$ and $Y_{\text{EGR}} = 0$ as well as $\dot{Q}_w = 600\text{W/cm}^2$ and $T_w = 450\text{K}$. All relevant values are calculated by a 1D flame simulation introduced in Sect. 4. The results are shown in Table 1. The inner layer formulation is less sensitive towards errors, especially concerning the unburned temperature.

3 Experimental setup and data processing

The direct observation and measurement of flame–wall interactions in a practical combustion device is a difficult task, as the requirements concerning spatial and temporal

resolution are very high. The quenching distance is commonly of order $\mathcal{O}(10\ \mu\text{m})$, while the duration of flame–wall interactions at elevated pressures and temperatures varies between 0.15–0.5 ms [25, 37]. Moreover, the measurement device has to be integrated in an environment with limited access to the combustion chamber, high temperatures and pressures as well as vibrations. As previously discussed, the wall heat flux is a characteristic quantity of flame–wall interactions which allows an estimation of the quenching distance in laminar as well as turbulent conditions. In combination with the normalised wall heat flux φ_Q and the corresponding Peclet number Pe_Q , flame–wall interactions can be assessed by comparing the results to the data published in literature. Highly resolved measurements of wall heat fluxes in engines have already been made numerous times [2, 13, 20, 39, 41] using the surface temperature method. The method proved to be robust enough to withstand the harsh measuring environment while retaining the necessary accuracy and response time. This makes it ideal for the evaluation of the flame–wall interaction process in a spark-ignition engine.

This section provides an overview of the experimental setup and programme before concluding with the evaluation of the wall heat fluxes.

3.1 Equipment and operating points

The engine used in the experiments is a three-cylinder BMW series production engine. It was modified to run on one cylinder only in order to integrate it in a conventional single-cylinder test bed. Charge air was supplied by an external compressor. Technical details are provided in Table 2.

The cylinder head of the engine was equipped with eight coaxial K-type surface thermocouples produced by the company Medtherm. According to the manufacturer, the time constant is of order $1\ \mu\text{s}$ due to the thin plating of approximately $2\ \mu\text{m}$. The thermocouples were mounted in aluminium sleeves and subsequently calibrated using a dynamic test rig described by Wimmer et al. [41]. Besides a correction of manufacturing tolerances, this approach also minimises the error due to heat conduction between the thermocouple and the sleeve. The assembled thermocouples

were then installed flush with the walls of the cylinder head. The locations of the measuring positions are shown in Fig. 1. The sensors were connected to the indication system via an analogue amplifier. Additionally, pressure indication in the cylinder as well as in the exhaust and intake ports was employed. The sampling interval of these quantities was 0.5° , which corresponds to a sampling frequency of 24 and 48 kHz at 2000 rpm respectively 4000 rpm. The duration of flame–wall interactions is expected to be in the range of $\mathcal{O}(0.15\ \text{ms})$ – $\mathcal{O}(0.5\ \text{ms})$ at elevated pressures [25, 37]. Hence, the time resolution is sufficient. The wall heat flux was calculated afterwards by solving a one-dimensional heat conduction equation. Details of this procedure can be found in the paper of Wimmer et al. [41]. For a meaningful statistical assessment, the indication system was set to capture 1000 consecutive cycles for each operating point. Furthermore, several other quantities such as the intake or the exhaust temperature, fuel flow and exhaust gas equivalence ratio were recorded and averaged over a 60 s measuring interval to provide additional data for the verification of the simulations.

The engine was operated at five different measuring points in order to examine the influence of speed, load, equivalence ratio and charge motion on the quenching process. In this way, a wide spectrum of different pressures, temperatures, mixture and flow properties during flame–wall interaction can be covered, which is important for a comprehensive evaluation. An overview of all operating points is given in Table 3. OP1 and OP2 are both full

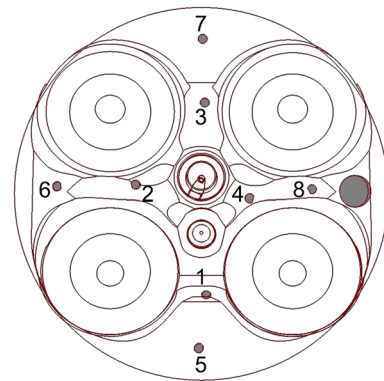


Fig. 1 Measuring positions in the cylinder head

Table 2 Engine specifications

Engine type	Gasoline, 4-stroke
Cylinders/valves per cyl.	1/4
Compression ratio	11.0
Displacement volume	499.6cm^3
Bore and stroke	$82 \times 94.6\ \text{mm}$
Valve train	Variable valve lift and timing
Combustion process	Direct injection, homogeneous charge

Table 3 Operating points

	Speed	Load (rpm)	IMP	Φ	Charge motion
OP1	2000	Full load	20 bar	1.0	Tumble
OP2	4000	Full load	20 bar	1.1	Tumble
OP3	2000	Part load	3 bar	1.0	Swirl
OP4	2000	Part load	3 bar	1.0	Tumble
OP5	2000	Full load	15 bar	0.7	Tumble

load points at different engine speeds whereas OP3 and OP4 are part load points which differ in the control strategy of the engine load: at OP3, the engine is throttled by an asymmetrical reduction of the intake valve lifts. This results in a swirling charge motion. At OP4, the intake pressure is reduced by a conventional throttle valve while retaining the maximum (symmetrical) valve lift. This leads to a tumbling motion at part load. OP5 is essentially a full load point with the same operating parameters as OP1 apart from the injected fuel mass which was reduced to examine flame–wall interactions at lean conditions.

3.2 Evaluation of wall heat fluxes

The combustion process in a modern spark-ignition engine is highly turbulent resulting in a significant cycle-to-cycle variation of the flame propagation and consequently of the wall heat flux. For example, wall heat flux traces of 50 consecutive cycles at OP1 and all measuring points are shown in Fig. 2. The evaluation of high-frequency phenomena such as flame–wall interactions, therefore, requires the analysis of single cycles.

The characteristic features of flame–wall interactions are a steep gradient attributed to the arrival of the flame and a subsequent maximum of the wall heat flux $\dot{Q}_{W,Q}$ associated to the moment of quenching. As one can see in Fig. 3, the single cycle trace exhibits both these features in contrast to the ensemble-averaged trace. For the analysis of the quenching process, the wall heat fluxes $\dot{Q}_{W,Q}$ as well as the corresponding crank angles α_Q have to be extracted from the single cycle traces for each measuring point. This was done by an algorithm which assessed and classified the individual traces for each cycle and measuring point. Only the individual wall heat flux traces exhibiting the earlier mentioned characteristics of flame–wall interactions were chosen for the analysis. The result of this analysis is shown exemplary for the measuring point 1 at operating point 1 in Fig. 4.

As one can see, there is a significant scatter of the data which can be attributed to varying mixture properties on the one hand and different flame orientations on the other hand. Unfortunately, the individual assessment of the quenching distance y_Q as well as of φ_Q and Pe_Q at each of these data points is not possible, as explained in the following section.

4 Simulative method for the analysis of the wall heat fluxes

Irrespective of the choice of correlation, i.e. (4) or (6), some important laminar flame characteristics, like s_L^0 , T_0 or T_b , have to be known to calculate the quenching distance.

These quantities can be calculated when the mixture properties, i.e. the pressure p , the unburnt temperature T_u , the equivalence ratio ϕ and the residual gas mass fraction Y_{EGR} in the moment of quenching are known. However, ϕ and T_u can exhibit significant spatial gradients and cycle-to-cycle variations in a direct-injected spark-ignition engine leading to the scatter of the quenching wall heat fluxes as shown in Fig. 4. Thus, an estimation of these values solely based upon a zero dimensional representation of the combustion chamber is insufficient. A possible solution for this problem is utilizing a 3D URANS-CFD simulation of the in-cylinder flow. In this case, however, cycle-to-cycle fluctuations can still not be resolved since the underlying equations are implicitly averaged. This issue persists even if a numerical method capable of resolving single cycles, like LES, is employed, since an unambiguous assignment of simulation and experiment is not possible. For example, cycle 25 from LES does not necessarily represent cycle 25 from experiment. Hence, an accurate assessment of the quenching distances of individual cycles is not possible. However, an evaluation of the mean quenching distances can be done. For this purpose, the previously estimated individual wall heat fluxes in the moment of quenching are ensemble-averaged for each operating and measuring point. The result is the mean wall heat flux and point in time of quenching. The latter information can subsequently be used to estimate p , T_u , ϕ and Y_{EGR} using 3D-CFD. In a physical sense, the mean mode of flame–wall interaction is investigated at each operating and measuring point.

A complete overview of the simulative workflow is given in Fig. 5. The quality of the results of a 3D-CFD simulation depends on the prescribed initial and boundary conditions, which should be as accurate as possible. For this reason, a 1D gas exchange simulation as well as a complete thermal analysis was conducted for each operating point. The latter comprises an iterative succession of 3D-CFD in-cylinder and coolant flow as well as 3D-FE heat transfer simulations to provide a spatially resolved wall temperature. The 1D gas exchange simulation was conducted with GT Power and subsequently used to calculate the necessary mass flow, pressure and temperature boundary conditions. All 3D-CFD calculations were made with the commercial CFD software FIRE by AVL, whereas Simulia Abaqus was used as the 3D-FE tool. All simulations were validated and showed a satisfactory agreement compared to the available experimental data.

Having estimated the basic state variables p , T_u , ϕ and Y_{EGR} in the moment of quenching at each measuring location individually for each operating point by 3D-CFD simulation, the calculation of the laminar flame properties, such as s_L^0 , l_F and T_0 , is now feasible. For this purpose, 1D

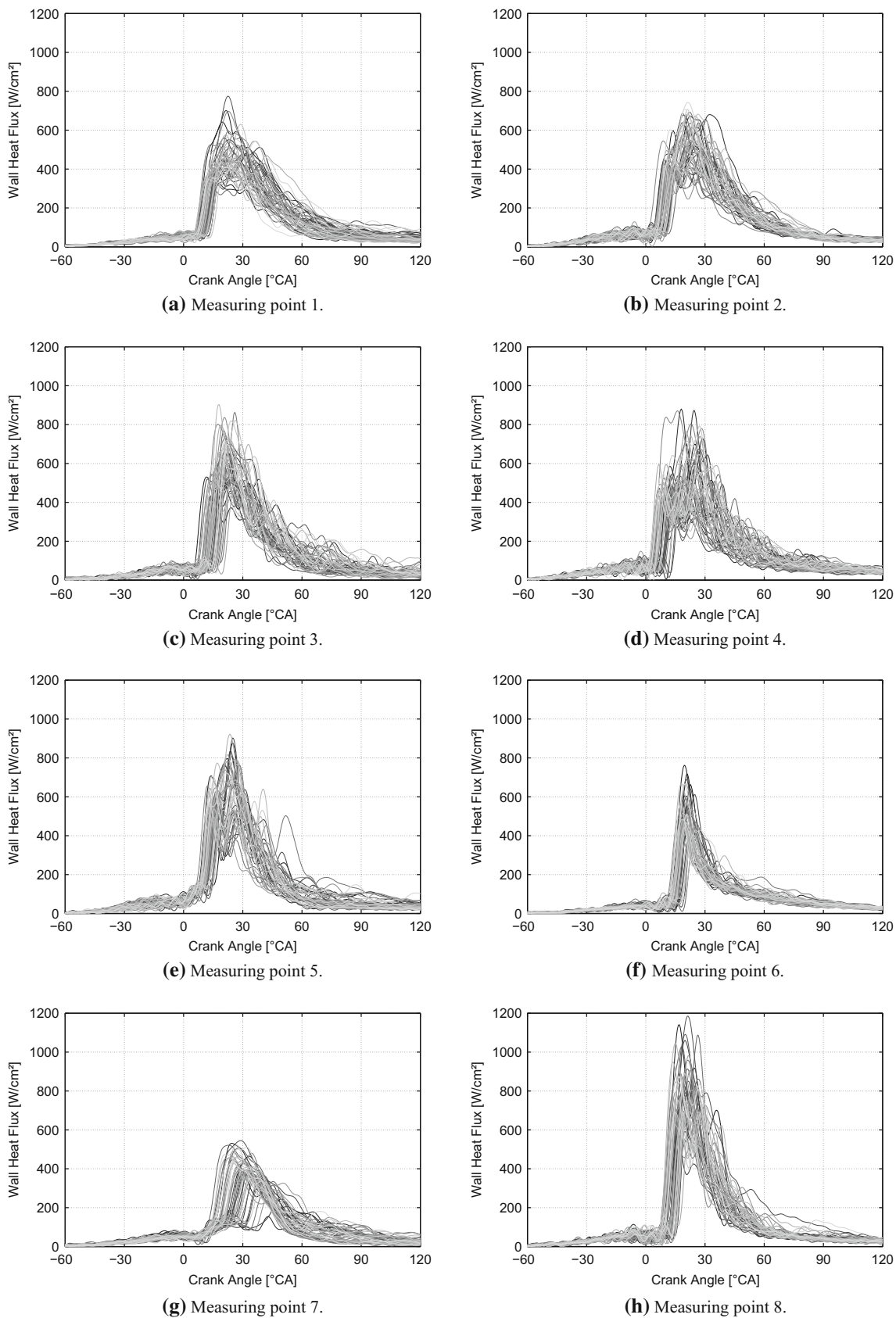


Fig. 2 Wall heat flux traces of 50 consecutive cycles at OP1 and all measuring points

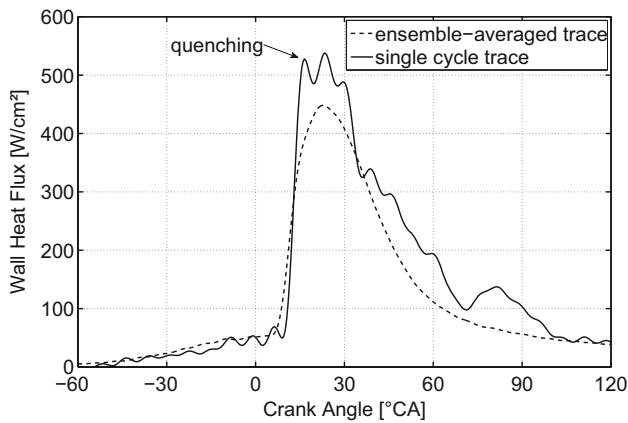


Fig. 3 Wall heat flux traces at OP1 and measuring point 1

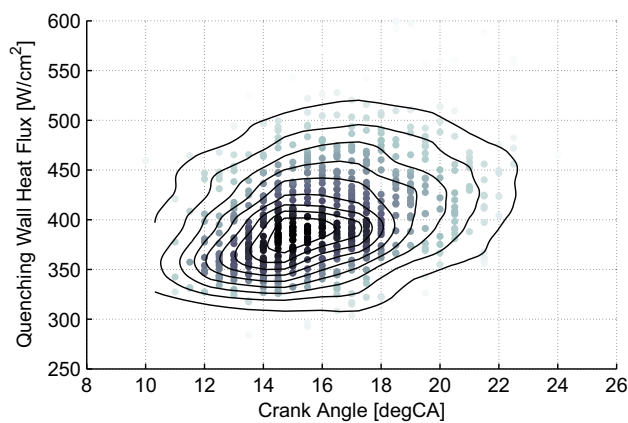


Fig. 4 Scatter plot of the wall heat fluxes in the moment of quenching at OP1 and measuring point 1. For clarity, the datapoints are colored based upon the corresponding probability density. Moreover, a contour plot of the probability density is also shown

(free) flame calculations were conducted using the open-source software Cantera. The most critical aspect in this respect is the choice of the reference fuel as well as the

reaction mechanism. The experiments were conducted using gasoline with an addition of 10.5% ethanol. In order to emulate the behaviour of the real fuel, a surrogate fuel comprising 43.07 vol% iso-octane, 13.91 vol% *n*-heptane, 32.52 vol% toluene and 10.50 vol% ethanol was estimated using a correlation by Cai et al. [12]. The H/C-ratio, the air requirement as well as the lower heating value are summarized in Table 4. The reaction mechanism employed was also developed by Cai et al. and validated against ignition delay times and laminar flame velocities available in literature [12].

At this point, all required input quantities for the correlations (4) and (6) are known and the quenching distance as well as the normalised scales can be calculated and used to assess the flame–wall interactions in a spark-ignition engine.

5 Results and discussion

In the following, the results of the previously described analysis are presented and discussed. It has to be noted that at OP2, the measuring points 2 and 7 were excluded due to disturbances in their output signal. In general, the duration of the observed flame–wall interactions ranges between 0.15 and 0.4 ms, which is in good accordance with the laminar quenching duration of stoichiometric methane air-flames at elevated pressures reported by Sotton et al. [37] and Labuda et al. [25]. To fully examine the quenching process in a spark-ignition engine, the quenching distance as well as the normalised scales are discussed below.

5.1 Quenching distances

The mean quenching distances y_Q estimated with the inner layer formulation (6) at each operating point are shown in

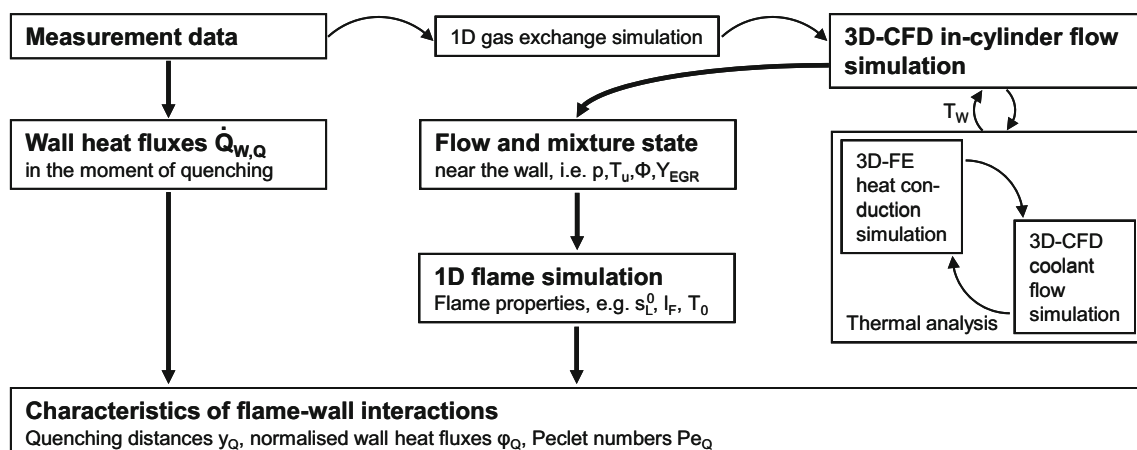


Fig. 5 Overview of the complete workflow including all simulative tasks

Table 4 Fuel characteristics

	Fuel	Surrogate
H/C-ratio	1.86	1.83
Air requirement (kg/kg)	13.93	13.86
Lower heating value (MJ/kg)	41.87	41.21

Fig. 6a. The large crosses represent the average of all measuring points at a specific operating point. The order of magnitude of the quenching distance in spark-ignition engines is 15–100 μm .

A few general statements can already be deduced by comparing the different operating points. The variation of speed (OP1 vs. OP2) has less influence on the quenching distance than the variation of the load (OP1 vs. OP4). Lean combustion exhibits larger quenching distances than stoichiometric combustion (OP1 vs. OP5). However, a general scheme can not be deduced by comparing the quenching distances to the operating conditions of the engine given in Table 3.

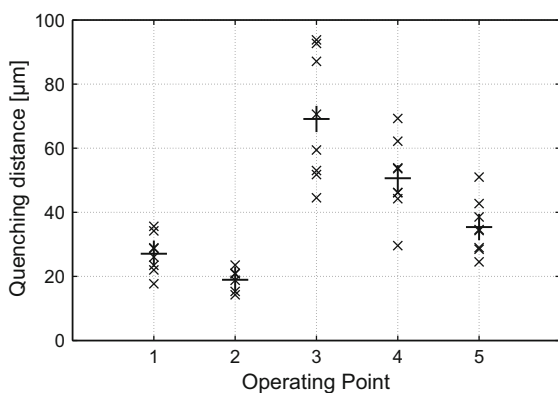
To find appropriate explanations for these phenomena, the flame characteristics and in particular the laminar flame thickness have to be considered. If the flame thickness is small, the flame can propagate closer to the wall without being influenced by wall heat losses. A wider laminar flame, in contrast, starts to interact with the wall at a higher distance yielding a higher quenching distance. This relation can be illustrated by comparing the quenching distances to the laminar flame thicknesses l_F shown in Fig. 6b. The latter were calculated with Eq. (3) solely based upon the simulations described in the previous section. Both quantities exhibit the same trends indicating that the quenching distances in a spark-ignition engine are proportional to the laminar flame thickness at first order, i.e. $y_Q \sim l_F$. This is in accordance with the findings of the previously mentioned

studies on laminar flame–wall interaction which indicate that the Peclet number $Pe = y_Q/l_F$ (Eq. 2) is approximately constant for a given quenching configuration (HOQ or SWQ).

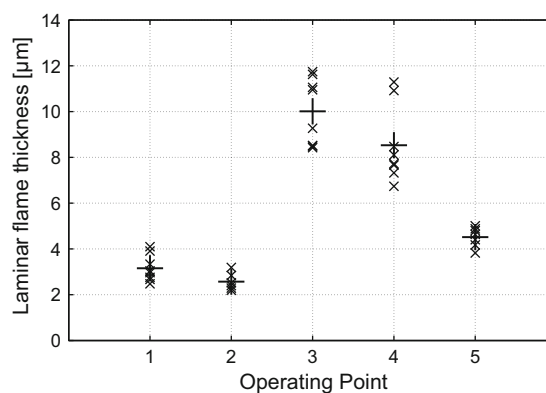
Thus, the influence of different operating parameters on the quenching distance can be discussed by questioning their effect on the laminar flame properties. A higher load, for example, leads to an increased in-cylinder pressure p , directly lowering the laminar flame thickness l_F and the quenching distance y_Q . Lean combustion increases the laminar flame thickness l_F and the quenching distance y_Q in turn. The engine speed as well as the charge motion have an indirect effect as they mainly affect the mixture homogenisation and hence, the local equivalence ratio ϕ .

However, the most important parameter regarding the quenching distance is found to be the in-cylinder pressure, which is directly coupled to the engine load. This can be explained as follows: in contrast to the in-cylinder pressure, the fresh gas temperature as well as the equivalence ratio are mainly determined by the engine design. The former depends on the compression ratio, whereas the latter usually ranges within a small operating window defined by the exhaust gas aftertreatment or the emission regulations. In the present study, the pressure varied between 15 and 90 bar whereas the unburned temperature and the equivalence ratio varied between 800 and 880 K respectively 0.85–1.15 (with the exception of OP5). Therefore, a further discussion of the quenching distance in terms of its pressure dependence is sensible.

Comparison of the inner layer formulation and the relation by Boust The quenching distances obtained with the inner layer formulation (6) and the relation by Boust (4) are plotted against the pressure during quenching in Fig. 7. To clarify the trends, a least-square fit of the commonly chosen scaling law $a \times p^b$ is also included.



(a) Quenching distances y_Q evaluated with the inner layer formulation (6) at each operating and measuring point.



(b) Laminar flame thicknesses l_F in the moment of quenching evaluated by simulation at each operating and measuring point.

Fig. 6 Obtained quenching distances and laminar flame thicknesses. Each small cross represents the mean result at a measuring point, whereas the large cross visualizes the average of all measuring points

The quenching distances estimated with the inner layer formulation are generally smaller than those estimated with the relation by Boust. The reason for this is the different definition of the flame position. In the former, the flame is uniquely identified by the location of the inner layer whereas in the latter, the flame position was defined by the chemiluminescence of methane-air flames in the visible spectrum (mainly CH^* and C_2^*). Therefore, both relations are not directly comparable as the emission peak of CH^* and C_2^* does not, in general, coincide with the position of the inner layer. Nevertheless, both relations exhibit the same behaviour. Based on these results, a first order approximation of the quenching distance in spark-ignition engines operated with gasoline fuels reads

$$y_Q \approx 280 \mu\text{m} \times (p/1\text{bar})^{-0.55}. \quad (7)$$

The pressure scaling of $p^{-0.55}$ compares well to the theoretical scaling of the laminar flame thickness for stoichiometric gasoline-air mixtures $l_F \sim p^{-0.65} T_u^{-1.55}$ which was obtained by 1D flame calculations of the surrogate fuel. This again indicates that the quenching distance y_Q is directly related to l_F . Note that the scaling of l_F is only valid for stoichiometric mixtures. If the lean operating point 5 is excluded for this reason, the pressure scaling of the experimental quenching distances becomes $p^{-0.6}$, which is in good agreement with the theoretical prediction considering the neglected variations of T_u , ϕ and Y_{EGR} . Moreover, the pressure exponent compares well against the reported values in literature, which range from -0.48 [25], -0.51 [37], -0.56 [40] for stoichiometric methane-air mixtures to -0.88 [40] for stoichiometric methanol-air mixtures.

Comparison to literature To assess the flame-wall interaction process in a spark-ignition engine, it is useful to compare the quenching distances to the ones found in

literature. Unfortunately, to the best of the author's knowledge, there is only one study (Labuda et al. [25]) investigating laminar flame quenching at comparable conditions like the present work. The authors examined the head-on quenching process of stoichiometric methane-air flames at pressures between 8 and 160 bar and unburnt temperatures of around 800–850 K. These conditions compare favourably to the present study. Moreover, they also utilized the highly resolved measurement of wall heat fluxes as well as the relation by Boust et al. (4) to calculate the quenching distances. Hence, a comparison to the quenching distances in a spark-ignition engine obtained by Eq. (4) is feasible, since the definition of the flame position is identical in both cases.

However, the quenching distances estimated by Labuda et al. [25] have to be adapted to the laminar flame thickness of gasoline. For a pressure between 20 and 80 bar and an unburnt temperature of 800 K, it can be found by 1D flame calculations that the diffusive flame thickness of methane-air mixtures is larger by a factor of 1.7 compared to the flame thickness of gasoline-air flames, i.e. $l_{F,\text{CH}_4}/l_{F,\text{g}} = 1.7$. Since the quenching distance is proportional to the flame thickness l_F at first order, the head-on quenching limit of the quenching distance of stoichiometric gasoline-air flames can be found by scaling the results of Labuda et al. by $l_{F,\text{g}}/l_{F,\text{CH}_4}$. The side-wall quenching limit can be estimated by multiplying this results with a factor of 3 as discussed in Sect. 2. These limits are now representative for the laminar quenching distances of stoichiometric gasoline-air mixtures. As one can see in Fig. 8, the obtained quenching distances lie between these two limits indicating that flame-wall interactions in spark-ignition engines are essentially laminar.

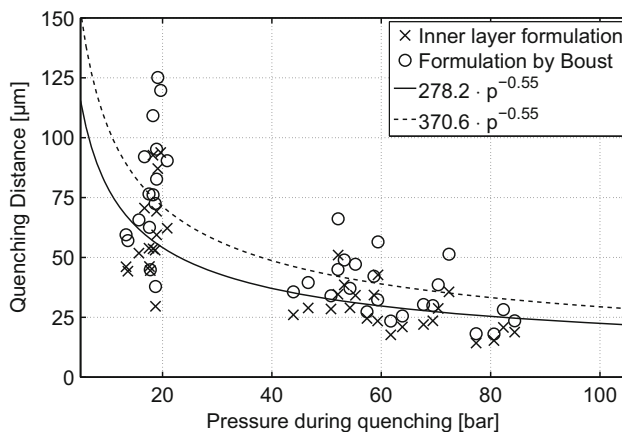


Fig. 7 Comparison of the quenching distances obtained with the relations (4) and (6) at all operating and measuring points. The pressure scaling is highlighted by least-square fits of the exponential equation $a \times p^b$

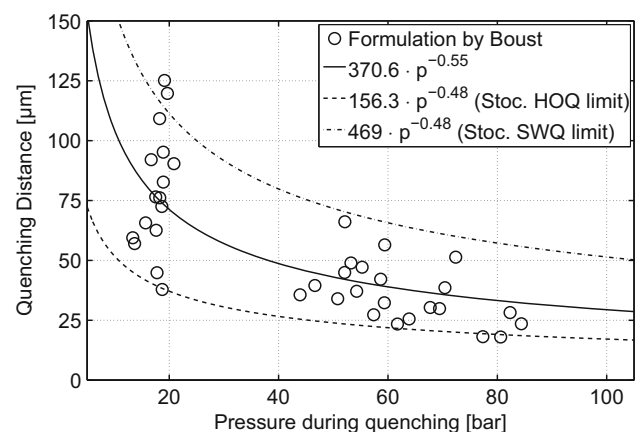


Fig. 8 Comparison between the quenching distances obtained with relation (4) and the predicted limits for laminar HOQ/SWQ of stoichiometric gasoline-air flames

5.2 Normalised wall heat fluxes and Peclet numbers

Further clues about the nature of flame–wall interactions in spark-ignition engines can be found by analysing the normalised wall heat fluxes φ_Q and the Peclet numbers Pe_Q . For laminar quenching, these quantities remain within certain bounds, as discussed in Sect. 2. If flame–wall interactions in spark-ignition engines are laminar, as suggested by the analysis of the quenching distances, the same is expected of the present values of φ_Q and Pe_Q .

Normalised wall heat fluxes The normalised wall heat fluxes φ_Q estimated with equation (1) are shown in Fig. (9). The highlighted areas correspond to the expected values for laminar HOQ and SWQ. As one can see, all values except for one at OP3 lie within the bounds defined by laminar flame–wall interactions. This outlier results from a locally rich mixture near the flammability limit. Hence, small errors in the estimate of the equivalence ratio result in large differences in the calculation of the flame power.

Despite the large variations between the operating points regarding mixture properties, charge motion and quenching distance, the normalised wall heat fluxes are comparable. This indicates that the underlying processes of quenching are similar at the examined operating conditions. This strongly supports the assumption that the quenching process of flames in spark-ignition engines is thermally controlled and similar to laminar flames. A flame in a spark-ignition engine is quenched when it loses about 10–20% of its total power to the wall depending on the local orientation of the flame. The mean normalised wall heat flux is

$$\varphi_Q = 0.14 \tag{8}$$

meaning that the average quenching process in a spark-ignition engine is essentially a superposition of HOQ and SWQ.

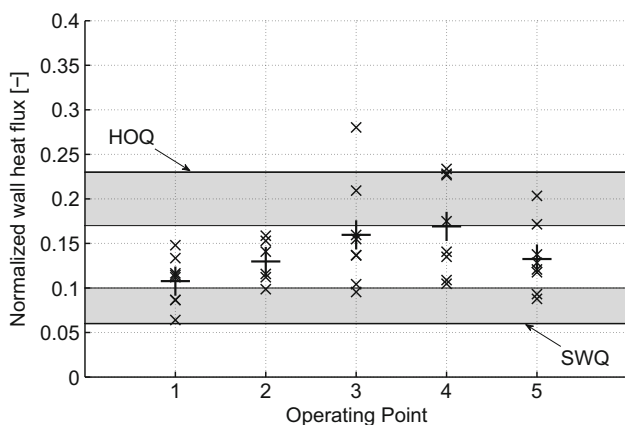


Fig. 9 Normalised wall heat flux φ_Q calculated by Eq. (1) at each operating and measuring point. The large crosses correspond to the average value at each operating point

At this point, it shall again be pointed out that the normalised wall heat fluxes φ_Q are the averaged wall heat fluxes during quenching. This means that they indicate the mean mode of flame–wall interaction at a specific location. As previously discussed, a cycle-resolved analysis is not possible in a meaningful way. In this context, turbulence does play a role, since it determines the degree of wrinkling and thereby the local orientation of the flame during quenching. If the turbulence is high, it can be expected that the local flame orientation exhibits a large cycle-to-cycle variance resulting in an average flame–wall interaction mode between HOQ and SWQ. If it is low in contrast, this effect is less pronounced and it is more likely that the mean mode at one location converges to either HOQ or SWQ. This role of turbulence can be seen by comparing the scatter of φ_Q at OP2 and OP3. OP2 possesses the highest turbulence level and the lowest degree of scattering, whereas OP3 has the lowest turbulence level and the highest degree of scattering. This explanation also applies to the differences in the degree of scattering of the quenching distances (Fig. 6) at the operating points. As the quenching distance also depends on the mixture properties at each measuring location in contrast to φ_Q , turbulence does also possess a secondary effect in this case: the higher it is, the better the mixture homogenisation and the lower the spatial differences between each measuring locations.

Peclet numbers The Peclet numbers were estimated by normalising the quenching distances evaluated with the inner layer formulation according to equation (2). The thermal conductivity λ and the specific heat c_p were chosen in accordance with Eq. (6) respectively (1). The results are shown in Fig. 10. Again, the highlighted areas correspond to the limiting cases of laminar quenching. All values of Pe_Q lie within the bounds of laminar flame–wall

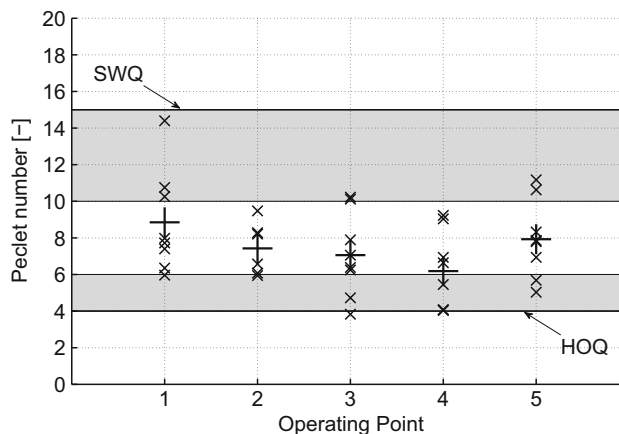


Fig. 10 Peclet numbers Pe_Q of the quenching distances calculated with the inner layer formulation at each operating and measuring point. The large crosses correspond to the average value at each operating point

interactions. This behaviour can be expected based upon the previous discussion of the normalised wall heat fluxes φ_Q since both quantities are inversely correlated. The mean Peclet number is

$$Pe_Q \approx 7.7. \tag{9}$$

Based upon this relation, a more sophisticated approach of estimating the quenching distance including mixture property variation can be developed using Eq. (2):

$$y_Q = l_F \times Pe_Q = \frac{\lambda}{\rho_u c_P s_L^0} Pe_Q. \tag{10}$$

In this context, the Peclet number Pe_Q can also be adapted to the local flame orientation. Sound assumptions for HOQ as well as SWQ are $Pe_{Q,HOQ} \approx 5$ and $Pe_{Q,SWQ} \approx 10$, respectively.

Dependance on mixture properties For laminar flame-wall interactions, the normalised scales φ_Q and Pe_Q do not exhibit any evident dependency on mixture properties despite a slight pressure dependence (cf. [21, 25, 37]). Hence, a similar behaviour can be expected for the present results. Since φ_Q and Pe_Q are closely related, an examination of one of these quantities is sufficient.

Figures 11, 12 and 13 show the normalised wall heat fluxes φ_Q as a function of p , ϕ and T_u , respectively. A small pressure dependency with decreasing wall heat fluxes towards higher pressures is evident. This is in accordance with the previously mentioned studies, although more data is needed for a final assessment. Concerning the dependency on the equivalence ratio ϕ as well as the unburned temperature T_u , no obvious correlation exists, which is again in good agreement with the studies on laminar flame-wall interactions.

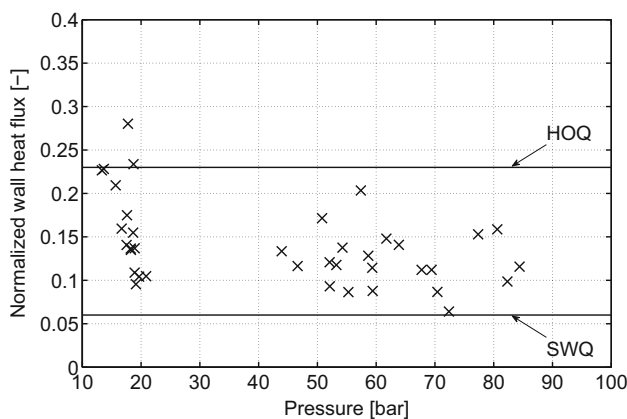


Fig. 11 Dependence of the normalised wall heat flux φ_Q on the pressure during quenching p . All operating and measuring points are depicted

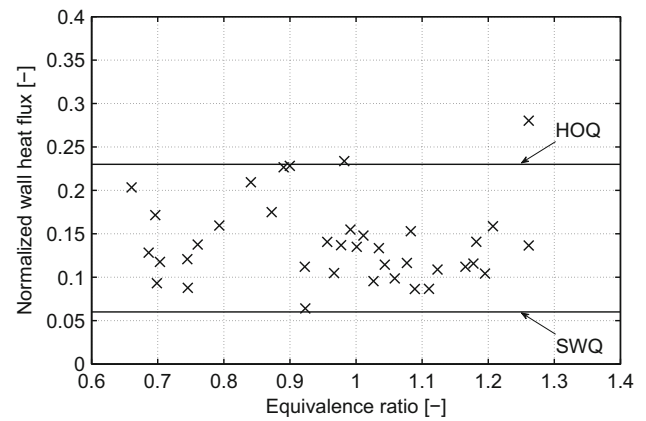


Fig. 12 Dependence of the normalised wall heat flux φ_Q on the local equivalence ratio ϕ . All operating and measuring points are depicted

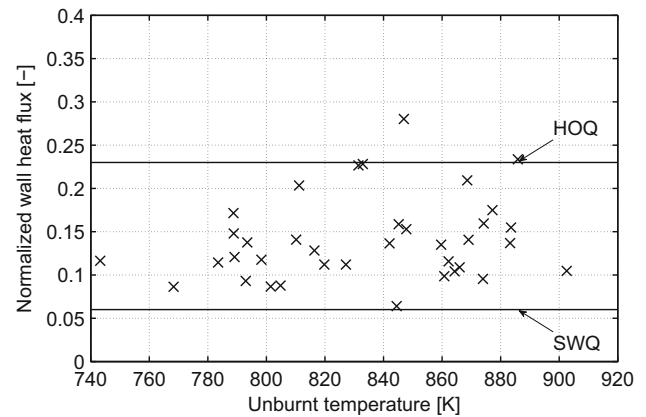


Fig. 13 Dependence of the normalised wall heat flux φ_Q on the local unburned temperature T_u . All operating and measuring points are depicted

5.3 Remarks and limitations

Although the diameter of the surface thermocouples is very small, they do not provide a strict one-point measurement, especially during SWQ. This leads to an underestimation of the wall heat flux and to an overestimation of the quenching distance in this case. Second, the quenching process in a spark-ignition engine can not be seen as isobaric in contrast to the studied flame-wall interactions in literature. The influence of a pressure gradient during quenching has not yet been examined. To account for this problem at least in a minimal way, the pressure was averaged between the beginning and the end of the interaction. Thirdly, the URANS simulation of the in-cylinder flow can only be seen as a good approximation of reality. To begin with, the exact geometry of the engine is unknown due to inevitable manufacturing tolerances. Moreover, the charge motion, mixture formation and combustion are all affected by the models and the numerics

employed. Such effects were countered by properly validating the employed simulations. It is expected that the mentioned issues do only have a minor influence on the outcome.

6 Conclusion

To clarify the nature of flame–wall interactions in spark-ignition engines, highly resolved measurements of the wall heat fluxes at different operating conditions were made. The cycle-resolved data was subsequently processed to extract the wall heat fluxes in the moment of quenching. This quenching wall heat flux can be used to calculate the quenching distance as well as the normalised wall heat flux φ_Q and the normalised quenching distance Pe_Q . For this purpose, a new relation for the calculation of the quenching distance, the inner layer formulation, was introduced and compared to the one proposed by Boust et al. [6]. To use either of these relations, the flow and mixture conditions near the wall in the moment of quenching have to be known. Hence, a simulative methodology was subsequently introduced to estimate these values with sufficient accuracy. The boundary and initial conditions were calculated using a 1D gas exchange analysis as well as a thermal analysis employing a succession of 3D-CFD in-cylinder flow, 3D-FE heat conduction and 3D-CFD coolant flow simulations. Based upon the final 3D-CFD in-cylinder flow calculation, a 1D simulation of a freely propagating flame with detailed chemical kinetics was conducted to provide the necessary laminar flame properties such as s_L^0 .

The analysis of the quenching distances revealed that they depend on mixture properties, which are influenced by the engine operating parameters. In this respect, the pressure being determined by the engine load is the parameter of leading order. Furthermore, it was shown that the quenching distances are comparable to the ones published in literature for laminar flame–wall interactions despite the varying operating conditions. The normalised wall heat fluxes φ_Q and Peclet numbers Pe_Q exhibited a similar behaviour and the same order of magnitude as during laminar quenching. This experimental evidence strongly supports the initial assumption that flame–wall interactions in spark-ignition engines are essentially laminar. Thus, the processes which lead to quenching, i.e. radical recombination and termination of the chain branching reactions due to heat losses, can also be assumed to be similar. Hence, the insights provided by previous studies on laminar flame quenching can also be utilized in the context of internal combustion engines. Moreover, the results provide experimental evidence for the flamelet hypothesis as well as for the assumption that the late stage of combustion near the

cylinder walls is laminar. It can be expected that the observed behaviour of flame–wall interactions is the same for all types of internal combustion engines with a premixed combustion process.

The typical scales of quenching in spark-ignition engines for a wide array of operating conditions read:

$$\varphi_Q \approx 0.14, \quad (11)$$

$$Pe_Q \approx 7.7, \quad (12)$$

$$y_Q \approx 280 \mu\text{m} \times (p/1\text{bar})^{-0.55}. \quad (13)$$

Note that the last relation is only valid for gasoline-air mixtures. For other fuels it has to be scaled with the ratio of the corresponding diffusive flame thicknesses $l_F/l_{F,g}$. The results of this study suggest that a more detailed estimation of the quenching distance including the variation of mixture properties is possible by simply assuming $Pe_Q = \text{const}$. A comprehensive quenching distance estimation can thus be made by

$$y_Q = \frac{\lambda}{\rho_u c_p s_L^0} Pe_Q \quad (14)$$

where Pe_Q can either be assumed to be constant ($Pe_Q = 7.7$) or dependant on the local flame orientation, i.e. Pe_Q varies between $Pe_{Q,HOQ} = 5$, respectively, $Pe_{Q,SWQ} = 10$. This relation is valid for all fuels and types of internal combustion engines with premixed combustion.

The presented results can be used to develop or adapt combustion models for premixed combustion in the future, aiding the design and optimisation of efficient engines.

Acknowledgements Open access funding provided by Graz University of Technology.

Open Access This article is distributed under the terms of the Creative Commons Attribution 4.0 International License (<http://creativecommons.org/licenses/by/4.0/>), which permits unrestricted use, distribution, and reproduction in any medium, provided you give appropriate credit to the original author(s) and the source, provide a link to the Creative Commons license, and indicate if changes were made.

References

- Alharbi, A.Y., Sick, V.: Investigation of boundary layers in internal combustion engines using a hybrid algorithm of high speed micro-PIV and PTV. *Exp. Fluids* **49**, 949–959 (2010)
- Alkidas, A.C.: Heat transfer characteristics of a spark-ignition engine. *J. Heat Transf.* **102**, 189–193 (1980)
- Alkidas, A.C.: Combustion-chamber crevices: the major source of engine-out hydrocarbon emissions under fully warmed conditions. *Prog. Energy Combust.* **25**, 253–273 (1999)
- Alshaaalan, T.M., Rutland, C.J.: Turbulence, scalar transport, and reaction rates in flame-wall interaction. *Symp. (Int.) Combust.* **27**, 793–799 (1998)

5. Alshaalan, T.M., Rutland, C.J.: Wall heat flux in turbulent premixed reacting flow. *Combust. Sci. Technol.* **174**, 135–165 (2002)
6. Boust, B., Bernard, L., Sotton, J., Labuda, S.A., Bellenoue, M.: A model of flame quenching in non-isothermal initial conditions. In: *Proceedings of the European Combustion Meeting* (2009)
7. Boust, B., Sotton, J., Labuda, S.A., Bellenoue, M.: Simultaneous measurements of laminar head-on quenching distance and wall heat flux for methane-air mixtures. In: *Proceedings of the European Combustion Meeting* (2005)
8. Boust, B., Sotton, J., Labuda, S.A., Bellenoue, M.: A thermal formulation for single-wall quenching of transient laminar flames. *Combust. Flame* **149**, 286–294 (2007)
9. Bruneaux, G., Akselvoll, K., Poinot, T., Ferziger, J.H.: Simulation of a turbulent flame in a channel, pp. 157–174. In: *Proceedings of the Summer Program, Center for Turbulence Research* (1994)
10. Bruneaux, G., Akselvoll, K., Poinot, T., Ferziger, J.H.: Flame-wall interaction simulation in a turbulent channel flow. *Combust. Flame* **107**, 27–44 (1996)
11. Bruneaux, G., Poinot, T., Ferziger, J.H.: Premixed flame-wall interaction in a turbulent channel flow: budget for the flame surface density evolution equation and modelling. *J. Fluid Mech.* **349**, 191–219 (1997)
12. Cai, L., Pitsch, H.: Optimized chemical mechanism for combustion of gasoline surrogate fuels. *Combust. Flame* **162**, 1623–1637 (2015)
13. Chang, J., Güralp, O., Filipi, Z., Assanis, D., Kua, T.-W., Najt, P., Rask, R.: New heat transfer correlation for an HCCI engine derived from measurements of instantaneous surface heat flux. SAE Paper 2004-01-2996 (2004)
14. Connelly, L., Ogasawara, T., Lee, D., Greif, R., Sawyer, R.F.: The effect of wall temperature on stagnation and sidewall flame quenching and resulting heat transfer. Fall Meeting, The Combustion Institute/Western States Section, Stanford, CA, Paper No. WSCI 92-109 (1992)
15. Connelly, L., Ogasawara, T., Lee, D., Greif, R., Sawyer, R.F.: Stagnation quenching of laminar, methane-air flames in a constant volume chamber: wall temperature effects. In: Fall Meeting, The Combustion Institute/Western States Section, Stanford, CA, Paper No. WSCI 93-077 (1993)
16. Dahms, R., Felsch, C., Röhl, O., Peters, N.: Detailed chemistry flamelet modeling of mixed-mode combustion in spark-assisted HCCI engines. *Proc. Combust. Inst.* **33**, 3023–3030 (2011)
17. Enomoto, M.: Head-on quenching of a premixed flame on the single wall surface. *JSME Int. J. Ser. B* **44**, 624–633 (2001)
18. Ezekoye, O.A., Greif, R., Sawyer, R.F.: Increased surface temperature effects on wall heat transfer during unsteady flame quenching. *Symp. (Int.) Combust.* **24**, 1465–1472 (1992)
19. Gruber, A., Sankaran, R., Hawkes, E.R., Chen, J.H.: Turbulent flame-wall interaction: a direct numerical simulation study. *J. Fluid Mech.* **658**, 5–32 (2010)
20. Harigaya, Y., Fujio, T., Shigeharu, O., Hiroshi, T.: Surface temperature and wall heat flux in a spark-ignition engine under knocking and non-knocking conditions. SAE Paper 891795 (1989)
21. Hasse, C., Bollig, M., Peters, N.: Quenching of laminar iso-octane flames at cold walls. *Combust. Flame* **122**, 117–129 (2000)
22. Heywood, J.B.: *Internal combustion engine fundamentals*. McGraw-Hill (1988)
23. Huang, W.M., Vosen, S.R., Greif, R.: Heat transfer during laminar flame quenching: effect of fuels. *Symp. (Int.) Combust.* **21**, 1853–1860 (1988)
24. Karrer, M., Bellenoue, M., Labuda, S.A., Sotton, J., Makarov, M.: Electrical probe diagnostics for the laminar flame quenching distance. *Exp. Therm. Fluid Sci.* **34**, 131–141 (2010)
25. Labuda, S.A., Karrer, M., Sotton, J., Bellenoue, M.: Experimental study of single-wall flame quenching at high pressures. *Combust. Sci. Technol.* **183**, 409–426 (2011)
26. Linse, D., Hasse, C., Durst, B.: An experimental and numerical investigation of turbulent flame propagation and flame structure in a turbo-charged direct injection gasoline engine. *Combust. Theory Model.* **13**, 167–188 (2009)
27. Linse, D., Hasse, C., Durst, B.: Probability density function approach coupled with detailed chemical kinetics for the prediction of knock in turbocharged direct injection spark engines. *Combust. Flame* **161**, 997–1014 (2014)
28. Liu, K., Burluka, A.A., Sheppard, C.G.W.: Turbulent flame and mass burning rate in a spark ignition engine. *Fuel* **107**, 202–208 (2013)
29. Owston, R., Magi, V., Abraham, J.: A numerical study of thermal and chemical effects in interactions of n-heptane flames with a single surface. *Combust. Flame* **148**, 127–147 (2007)
30. Peters, N.: Kinetic foundation of thermal flame theory. In: Sirignano, W.A., Merzhanov, A.G., de Luca, L. (eds.) *Advances in combustion science: in Honor of Ya. B. Zel'dovich*, Progress in Astronautics and Aeronautics, vol. 173, pp. 73–91. American Institute of Aeronautics and Astronautics (1997)
31. Poinot, T., Haworth, D.C., Bruneaux, G.: Direct simulation and modeling of flame-wall interaction for premixed turbulent combustion. *Combust. Flame* **95**, 118–132 (1993)
32. Poinot, T., Veynante, D.: *Theoretical and Numerical Combustion*, 3rd edn. Thierry Poinot, Denis Veynante (2011)
33. Pope, S.B.: *Turbulent Flows*. Cambridge University Press, Cambridge (2000)
34. Popp, P., Baum, M.: Analysis of wall heat fluxes, reaction mechanisms, and unburnt hydrocarbons during the head-on quenching of a laminar methane flame. *Combust. Flame* **108**, 327–348 (1997)
35. Popp, P., Smooke, M., Baum, M.: Heterogeneous/homogeneous reaction and transport coupling during flame-wall interaction. *Symp. (Int.) Combust.* **26**, 2693–2700 (1996)
36. Schmitt, M.: *Direct numerical simulations in engine-like geometries*. PhD thesis, ETH Zürich (2014)
37. Sotton, J., Boust, B., Labuda, S.A., Bellenoue, M.: Head-on quenching of transient laminar flame: heat flux and quenching distance measurements. *Combust. Sci. Technol.* **177**, 1305–1322 (2005)
38. Vosen, S.R., Greif, R., Westbrook, C.K.: Unsteady heat transfer during laminar flame quenching. *Symp. (Int.) Combust.* **20**, 75–83 (1985)
39. Wendland, D.W.: The effect of periodic pressure and temperature fluctuations on unsteady heat transfer in a closed system. NASA Report No. CR - 72323 (1968)
40. Westbrook, C.K., Adamczyk, A.A., Lavoie, G.A.: A numerical study of laminar flame wall quenching. *Combust. Flame* **40**, 81–99 (1981)
41. Wimmer, A., Pivec, R., Sams, T.: Heat transfer to the combustion chamber and port walls of IC engines—measurement and prediction. SAE Paper 2000-01-0568 (2000)